Tilt Rotor Aeromechanics Phenomena in Low Speed Flight

Mark A. Potsdam
US Army Aviation and Missile Research, Development and Engineering Center (AMRDEC), Army/NASA Rotorcraft Division, Aeroflightdynamics Directorate, Moffett Field, CA
mark.potsdam@us.army.mil

Mark J. Silva
Naval Air Systems Command (NAVAIR), Advanced Aerodynamics Branch, Air Vehicle Department, Patuxent River, MD
mark.silva@navy.mil

Abstract

This work investigates important aeromechanics phenomena affecting the V-22 tilt rotor in low speed sideward flight or while hovering in quartering or crosswind conditions. These phenomena, such as pitch-up with sideslip and increased power required in sideward flight, were identified during V-22 critical azimuth flight testing and impacted handling qualities in this flight regime. High fidelity, dynamic, unsteady, Navier-Stokes computational fluid dynamics (CFD) calculations are presented and compared with flight test data. CFD predicts the flight test trends as a function of wind direction, in good agreement with data. Detailed investigation clearly shows the interaction of the rotor wake with the airframe as the major cause of the aeromechanics phenomena seen on the V-22. Identification of the underlying flowfield physics allows investigation of options for alleviation and prediction of future tilt rotor configurations.

Notation

C_M	pitching moment coefficient, $M_Y/\rho(\Omega R)^2\, 2\pi R^3$
C_Q	rotor torque coefficient, $Q/\rho(\Omega R)^2\, \pi R^3$
C_T	rotor thrust coefficient, $T/\rho(\Omega R)^2\, \pi R^3$
DL/T	airframe download divided by total thrust
M_{tip}	tip hover tip Mach number
PUWSS	pitch-up with sideslip
R	rotor radius
TPP	tilt equivalent tip path plane tilt, $\sin^{-1}(C_M R/C_T \Delta z$
B	wind azimuth, degrees
Δz	vertical distance between CG and rotor hub
θ	blade collective angle at r/R = 0.75, 14 degrees
ρ	air density
Ω	rotor rotational speed

1. Introduction

Tilt rotor aircraft are recognized for their significant potential impact on both military and civilian aviation. The range and speed of a turboprop airplane is augmented by the ability to operate in and out of confined areas like a helicopter. For civilian operations this means reduced impact on an overloaded airspace system and reduced infrastructure costs. For military operations, increased payload and range with reduced aerial refueling operations are possible when compared with helicopters currently performing the same remote area missions. Taking advantage of the helicopter mode capability allows tilt rotors to hover in place, maneuver around an airfield at low speed, and conduct shipboard operations with wind over the deck. The V-22 Osprey is the first production military tilt rotor aircraft.

The objective of this work is to investigate important aeromechanics phenomena affecting the V-22 tilt rotor in operations requiring low speed flight in any direction or hovering in wind conditions. During V-22 critical azimuth flight testing designed to evaluate control margins and pilot workload under such flight conditions, phenomena such as pitch-up with sideslip (PUWSS) and increased power required in sideward flight were identified[1]. These phenomena adversely impacted handling qualities in this flight regime. Modifications to the flight control system were required in order to restore full control authority without reaching control limits in multi-axis maneuvers. These interactions are somewhat specific to the V-22 configuration, having not been seen, or perhaps recognized, on earlier tests of the XV-15[2].

In addition to the available V-22 flight test data, several experimental efforts have investigated rotor-airframe interactions on tilt rotor aircraft. The majority of this work, however, focused on no-wind hover.

McVeigh[3] investigated both no-wind and headwind hover conditions with no side winds. XV-15 flight testing[2] was performed for no-wind hover, sideward, and rearward flight. Previous computational work has shown that CFD can accurately predict both isolated tilt rotor performance and airframe loads for installed configurations in no-wind hover[4–6]. The present work extends earlier research to sidewind conditions.

2. V-22 Configuration

A computational model has been constructed of a V-22 airframe configuration in hover. The fuselage is the Full-Scale Development (FSD) configuration generated using high-fidelity V-22 fuselage, wing, nacelles, and tail geometry. The wing flaperon angle is set to 67 degrees in the CFD model, while flight test data were taken with a 72.5 degree setting. The rotor blade geometry is a representation of the NASA Tilt Rotor Aeroacoustics Model (TRAM) rotor[7]. The TRAM is an extensive wind tunnel model constructed to facilitate future tilt rotor aeromechanics research. The rotor geometry is a 0.25-scale 3-bladed V-22 rotor with geometric and dynamic scaling. The only geometric differences are in the blade cuff region inboard of 25% blade radius.

3. Critical Azimuth Testing

As part of the overall V-22 Osprey Engineering, Manufacturing and Development Program, handling qualities flight testing was performed to demonstrate, among other things, critical azimuth capabilities of the tilt rotor (Figure 1)[1]. Initial tests were conducted at sea level followed by high density altitude testing at light and heavy gross weights. Most conditions were flown using a pace vehicle. The V-22 was demonstrated in winds around the full 360° azimuth and speeds up to the 45 knots required by design specifications.

In critical azimuth flight testing, operational procedures affect the aircraft attitude and flight control positions, which are difficult to duplicate in a computational model. In flight the V-22 fuselage, nacelles, and rotors are controlled to maintain aircraft trim. In order to maintain balance, the pitch and roll attitude of the fuselage naturally varies throughout the wind azimuth envelope. Power is controlled to set rotor thrust in order to balance weight, download, and jet thrust. Control of the rotors through collective and lateral and longitudinal cyclic is used to maintain trim in side flight conditions. When approaching forward longitudinal stick limits, the nacelles are programmed to automatically transition forward to 85 degrees.

In the CFD calculations the fuselage pitch and roll attitudes are maintained at zero. The rotor collective angle, θ, is fixed at 14 degrees; therefore, the solutions are not trimmed to a constant thrust or weight. In spite of this, the total rotor thrust is relatively constant ($C_T \approx .015$ ±4%). Two hover tip Mach numbers (M_{tip}) were investigated. Maximum interim (continuous) power at sea level corresponds to a value of $M_{tip} = 0.736$ (104% Nr). A lower value of 0.625 (88% Nr) was also investigated corresponding to TRAM experiments. No rotor control cyclic inputs were specified. The nacelle angles are maintained at 90 degrees. No attempt was made to trim the aircraft in the various flight conditions.

4. Methodology

CFD calculations use the Reynolds-averaged Navier-Stokes code OVERFLOW-D[8]. It is based on the OVERFLOW 1.6au code, which has been continually developed at NASA and has been applied to a wide range of fluid dynamics problems. OVERFLOW-D includes major modifications for time-dependent, rigid body motion of components, in particular individual moving rotor blades. Solutions are computed on structured, overset grids using body-conforming "near-body" grids and Cartesian "off-body" grids in the wake and farfield.

For spatial discretization, OVERFLOW-D uses 4th-order central differencing with artificial dissipation. The time-accurate analysis uses an implicit 1st-order algorithm in the near-body grids and an explicit 3rd-order Runge-Kutta scheme in the off-body grids. The Baldwin-Barth one-equation turbulence model is used in the near-body grids, which are assumed fully turbulent. Off-body grids are modeled as inviscid in order to reduce numerical dissipation in the wake.

In the Chimera methodology, overset, structured near-body grids are generated about the geometry. The complete configuration, including the rotors, fuselage, and nacelles, is modeled as viscous. The near-body grids have sufficient resolution and extent to capture wall-bounded viscous effects. High resolution C-mesh topology blade grids are used.

Off-body Cartesian grid generation is automatically performed by OVERFLOW-D. The finest off-body spacing is 10% of the rotor tip chord. This level-1 off-body grid surrounds the rotors and the fuselage and captures the wake. Progressively coarser levels are generated out to the farfield boundary at 6.5 rotor radii from the center of the domain. Where grid points fall inside the geometry, hole cutting is employed to blank out these points. A streamwise cross-sectional cut through the volume grid system in Figure 3 shows the near-and off-body grids, hole cuts, and overlap for half the V-22 configuration. The total number of grid points in the full-span V-22 model is 47.6 million with 63% in the off-body grids. Details can be found in Reference 4.

Solutions are computed on parallel supercomputers (IBM, SGI, or Sun) or a network of Unix PCs/workstations communicating with the Message Passing Interface (MPI) protocol. Both the domain connectivity and flow solver modules have been parallelized for efficient, scalable computations using MPI[9]. Scalability of OVERFLOW-D on the 47.6 million point grid is illustrated in Figure 4 as speed up from a baseline, defined as 32 processors, and compared with ideal linear speed up. Due to efficient memory usage, up to 2 million grid points can be placed in 1 GB of memory, creating a lower limit of approximately 32 processors. Parallel efficiency typically falls off when the number of grid points per processor falls below 250,000, creating an upper limit of approximately 192 processors.

Simulations were run on 128 processors of either an IBM Power3 (375MHz) or Power4 (1.3 GHz) supercomputer. Use of 128 processors is seen to be a good compromise between speed (7.6 seconds per step) and efficiency (73%). Each rotor revolution requires 5 wallclock hours for 2400 iterations per revolution on the Power4. Domain connectivity accounts for 20% of the time.

5. Aeromechanics Phenomena

During V-22 critical azimuth testing, several aeromechanics phenomena were identified that adversely affected handling qualities. Independently, the phenomena have been recognized in CFD calculations, which have been particularly useful in detailing the causes of the phenomena[10]. In this work aeromechanics phenomena involving pitch-up with side slip (PUWSS) and increasing power in sideward flight will be addressed. They will be discussed in the context of 1) airframe download/thrust (DL/T) and equivalent tip path plane (TPP) tilt, 2) breakdown of airframe forces and moments by aircraft component (wing, fuselage, nacelle, sponsons, tail), 3) isolated fuselage characteristics, 4) trends with wind azimuth, and 5) trends with rotor tip speed. Figure 5 from V-22 critical azimuth flight testing[1] details the trends of several flight control parameters as a function of wind speed and direction.

6. Analysis and Discussion

OVERFLOW-D simulations were run for 0, 45, 90, 135, and 180 degrees wind azimuth at a 35-knot wind speed. Two hover tip Mach numbers (0.625 and 0.736) were investigated, as well as cases with rotors not turning. The baseline rotor speed is M_{tip} = 0.736. Calculations with winds were initiated from hover or nearby wind conditions. In general, 10 to 15 rotor revolutions are required to remove transients when parameters such as wind speed or direction are changed. Time-averaged results are averages over at least 5 rotor revolutions. Sample time histories of rotor performance and airframe forces are shown in Figures 6 and 7, respectively, for a 35-knot wind speed as a function of wind azimuth. Some conditions are steadier and would, therefore, have improved handling qualities. Major oscillations are 3 per rotor revolution due to the 3-bladed rotors.

6.1. Pitch-up with Sideslip.

PUWSS is a well-understood aeromechanics phenomenon in which the upwind rotor wake impinges on the horizontal tail causing the aircraft to pitch up[1]. The phenomenon is most critical with wind from ±45° azimuths, although it is seen in a range from 30 to 70 degrees. The pitching moment generated must be counteracted. Significant longitudinal stick displacement (longitudinal flapping), increased fuselage pitch attitude, and 85° nacelle tilt are evident in the flight test data (Figure 5) for quartering headwinds with speeds greater than 15 knots. The V-22 flight control system is programmed to tilt the nacelles forward 5 degrees automatically when longitudinal cyclic and flapping limits are approached in this condition. PUWSS was not documented for the XV-15. In the CFD calculations, PUWSS is noted as an increase in airframe pitching moment, CM, equilibrated to a TPP tilt (longitudinal flapping) required to counteract the moment. Equivalent TPP tilt is shown schematically in Figure 8 and determined from the following equation:

$$\text{TPP tilt} = \sin^{-1}(C_M R/C_T \Delta z)$$

Positive tip path plane tilt (flap down in front) counteracts a nose up pitching moment.

OVERFLOW-D time-averaged DL/T and equivalent TPP tilt are shown in Figure 9 for a 35-knot wind speed, with and without rotors. Note that the pitch-up is not indicated in the fuselage-only calculations, where the rotor motion has been turned off, indicating that this is an adverse rotor-airframe interaction. Calculated pitch-up trends are in excellent agreement with flight test measurements. Both show maximum pitch-up at the 45° wind azimuth with symmetric behavior about this azimuth. Outside the PUWSS region, in tailwind conditions with the wind azimuth greater than 90°, CFD predicts pitch-down characteristics. This correlates with the aft longitudinal stick, negative fuselage pitch attitude, and 95° nacelle tilt in flight test. The maximum pitching moment is increased by 17% as the hover tip Mach number is increased from 0.625 to 0.736. However, the equivalent TPP tilt is reduced by 14% for the higher tip Mach number. A minimum in TPP tilt occurs at a quartering 135° tailwind azimuth, although with

significantly reduced magnitude and consequences compared with the quartering headwind.

PUWSS is known to be due to the rotor wake impinging on the empennage. CFD flow visualizations confirm this as seen in Figure 10. In this image, extracted from a time-dependent animation, particles released from the upwind (left) blade tips impact on the aft fuselage and empennage. Additionally, a breakdown of the time-averaged DL/T and TPP tilt by airframe component in Figure 11 indicates that the majority of the pitch-up does indeed come from the tail as well as the fuselage.

Instantaneous, albeit representative, pressure forces in the download direction, shown in Figure 12 as a function of wind azimuth, are further indication of the decreased lift (increased download) on the tail and aft cargo ramp. Blue coloring on the configuration indicates upload while red indicates download. Comparing the 0° head and 90° sidewind cases with the 45° quartering wind, reduced upload on the tail upper surface and increased download on the tail lower surface and fuselage underside translate into the pitch-up.

To reduce the exposed area of the horizontal tail and increase its lift, the elevator was deflected 60 degrees down as shown in Figure 13. The nose up moment is reduced by 25% or 1.5° of equivalent TPP tilt. The reduction in pitching moment comes solely from the tail contribution.

6.2. Increasing Power in Sideward Flight.

Increased power requirements in sideward flight were revealed in V-22 EMD critical azimuth testing. It is seen in Figure 5 that power required (mast torque) to hover in sidewinds is 10–20% higher than no/low-wind hover. In constant high wind conditions the power required to hover increases drastically (up to 80%) as the wind direction moves from a headwind towards a sidewind. CFD clearly shows this to be an adverse rotor-fuselage interaction due to an increase in airframe download. There may also be adverse rotor-on-rotor interference.

The increase in power required in sideward flight can be directly correlated with an increase in download. Download over thrust trends in Figure 9 indicate increasing DL/T as wind azimuth is increased up to the sidewind condition. Further, increasing to 135° azimuth results in a value similar to 45°. From 135° to 180° the DL/T is roughly constant. Although CFD calculations predict a download in a tailwind compared with the upload in a headwind, flight test data indicate the power required in these two conditions is approximately the same. These conditions may be especially sensitive to fuselage pitch attitude, which is not taken into account in the CFD. Dimensional download at 90° azimuth is increased by 25% as the hover tip Mach number is increased from 0.625 to 0.736. Non-dimensionally, the crosswind DL/T is reduced by 10% for the higher rotor RPM.

Based on the component breakdown in Figure 11 and the pressure forces in the download direction in Figure 12, it is seen that in a 35-knot headwind all parts of the airframe are lifting. As the wind passes through 45°, the upload on the wing upper surface and fuselage aft upper surface is reduced. At 90° the download due to the rotor wake on the wing upper surface is significant. The flat bottom lower surface of the fuselage also has a large influence. The suction on this surface steadily increases as the wind direction approaches 90°. While the download value at 135° is similar to 45°, in comparison, there is an increased contribution from the wing due to the rotor wake impinging on the wing upper surface and separation off the flap. There is a smaller contribution from the fuselage ramp.

With a tailwind, wing download remains larger than with a headwind. This is due to the wake and tilt rotor fountain remaining over the wing when rotor swirl velocities are in opposition to the oncoming flow. This effect is evident in Figure 14, which shows velocity magnitude contours in a streamwise plane through the aircraft center of gravity (CG) and a centerline plane for both 35-knot head and tailwinds. For this reason the tailwind case also shows significant unsteadiness in rotor and airframe forces compared with a headwind (Figures 6 and 7). As expected there is a significant increase in side force on the fuselage as the wind approaches 90° (Figure 7). The side force divided by thrust in a 35-knot direct crosswind is 0.105.

The increasing power in sideward flight phenomenon was not identified on the XV-15, possibly due to a more rounded fuselage shape. It is noted that for the V-22 calculations the unpowered airframe shows a trend of increased download with sidewind (Figure 9), but this phenomena is magnified by the rotor downwash impinging on the wing upper surface and causing additional suction on the fuselage lower surface. The consequences of this rotor-fuselage interaction are significant. Developing an experimental model that can be turned through 180° of sideslip without interfering with the fuselage flowfield is difficult. CFD calculations have shown this to be a tractable problem, implying that future fuselage shapes can be investigated provided rotor interactions are included.

7. Conclusions

Aeromechanics phenomena affecting the V-22 tilt rotor in low speed flight or while hovering in wind from varying azimuths have been investigated using computational fluid dynamics. Results have been compared with V-22 flight test data, although quantitative

comparisons were generally not possible. The following conclusions are made:

1. Pitch-up with sideslip is caused by an adverse interaction of the rotor wake impinging on the aft fuselage and empennage. It is not present in rotor-off fuselage characteristics. Large down elevator deflections mitigate the phenomenon.

2. Airframe pitch characteristics are in excellent agreement between CFD and flight test, with wind azimuth trends correctly captured, including maximum pitch-up at 45 degrees and pitch-down in tailwinds.

3. Increasing power in sideward flight is caused by significantly increased download on the wing upper surface and flat fuselage lower surface.

Overall, CFD is an effective tool for predicting complex rotor-airframe interactions on tilt rotor configurations in sideward flight for reduced risk in design and flight test. Complex aeromechanics phenomena can be best explained using a combination of airframe forces and moments and detailed flowfield visualization.

Acknowledgements

The computer resources of the Department of Defense High Performance Computing Modernization Program (HPCMP) Major Shared Resource Centers (MSRC) are gratefully acknowledged.

References

1. Klein, G., B. Roberts, and C. Seymour, "MV-22 Handling Qualities Flight Test Summary." American Helicopter Society 56th Annual Forum, Virginia Beach, VA, May 2000.

2. Arrington, W.L., M. Kumpel, R.L. Marr, and K.G. McEntire, "XV-15 Tilt Rotor Research Aircraft Flight Test Data Report, Volume II of V: Performance and Handling Qualities." *NASA CR 177406*, June 1985.

3. McVeigh, M.A., W.K. Grauer, and D.J. Paisley, "Rotor/Airframe Interactions on Tiltrotor Aircraft." American Helicopter Society 44th Annual Forum, Washington, DC, June 1988.

4. Potsdam, M.A. and R.C. Strawn, "CFD Simulations of Tiltrotor Configurations in Hover." American Helicopter Society 58th Annual Forum, Montreal, Canada, June 2002.

5. Poling, D.R., H. Rosenstein, and R.G. Rajagopalan, "Use of a Navier-Stokes Code in Understanding Tiltrotor Flowfields in Hover." *Journal of the American Helicopter Society*, Vol. 43, No. 2, April 1998.

6. Tai, T.C. and J. Vorwald, "Simulation of V-22 Rotorcraft Hover Flowfield." *AIAA Paper 93-4878*, 1993 AIAA International Powered Lift Conference, Santa Clara, CA, December 1993.

7. Johnson, W., "Calculation of Tilt Rotor Aeroacoustic Model (TRAM DNW) Performance, Airloads, and Structural Loads." *Proceedings of the American Helicopter Society Aeromechanics Specialists' Meeting*, Atlanta, GA, November 2000.

8. Chan, W.M., R.L. Meakin, and M.A. Potsdam, "CHSSI Software for Geometrically Complex Unsteady Aerodynamic Applications." *AIAA Paper 2001-0593*, 39th Annual Aerospace Sciences Meeting and Exhibit, Reno, NV, January 2001.

9. Meakin, R.L. and A.M. Wissink, "Unsteady Aerodynamic Simulation of Static and Moving Bodies Using Scalable Computers." *AIAA Paper 99-3302*, 14th AIAA Computational Fluid Dynamics Conference, Norfolk, VA, July 1999.

10. Potsdam, M.A., Schaller, D.F., Rajagopalan, R.G., and Silva, M.J., "Tilt Rotor Aeromechanics Phenomena in Low Speed Flight," American Helicopter Society 4th Decennial Specialists' Conference on Aeromechanics, San Francisco, CA, January 2004.

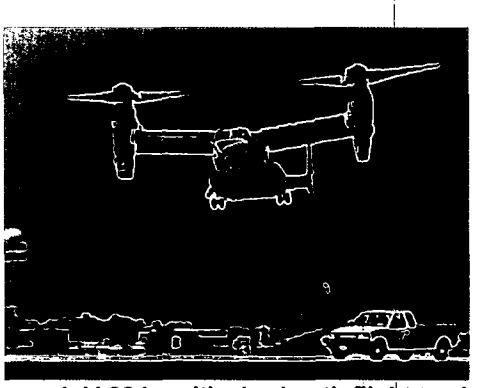

Figure 1. V-22 in critical azimuth flight testing

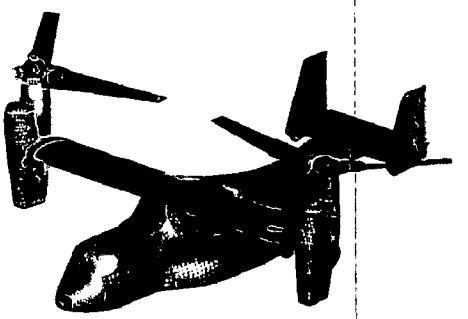

Figure 2. Shows the 109 V-22 near-body surface grids

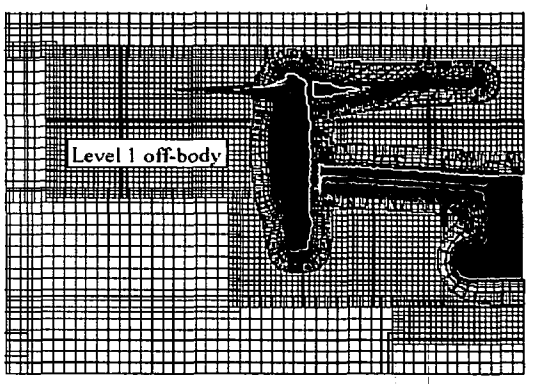

Figure 3. Slice through OVERFLOW-D volume grids (every third point)

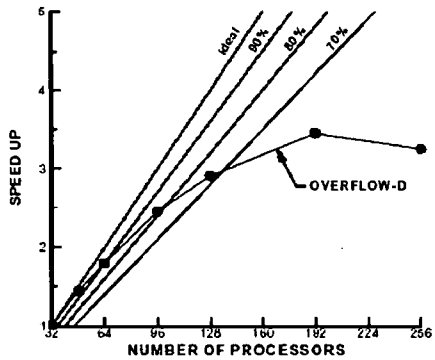

Figure 4. OVERFLOW-D parallel scalability

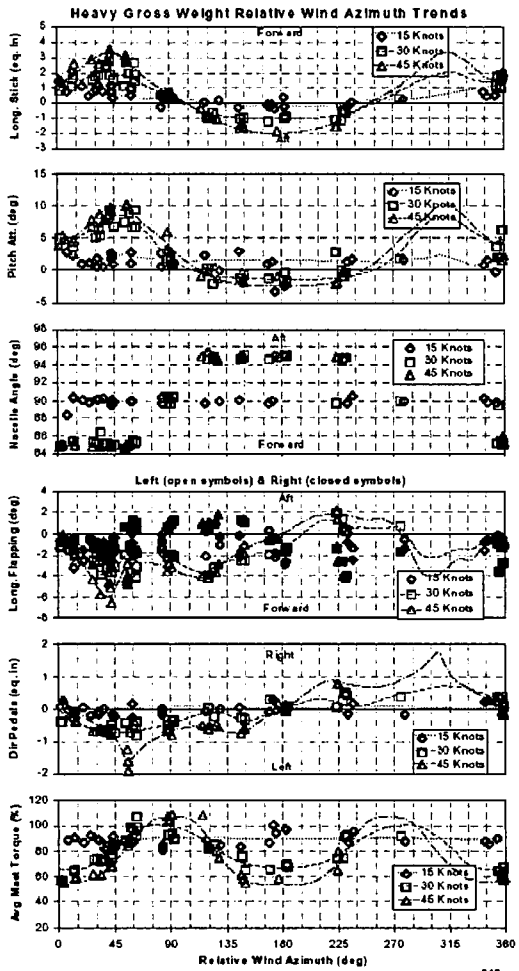

Figure 5. V-22 critical azimuth flight data[1]

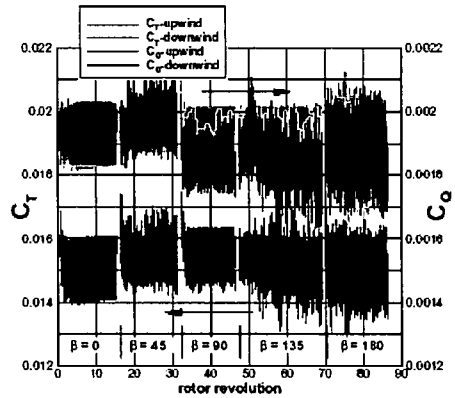

Figure 6. OVERFOW-D rotor performance time histories as a function of wind azimuth, 35-knot wind

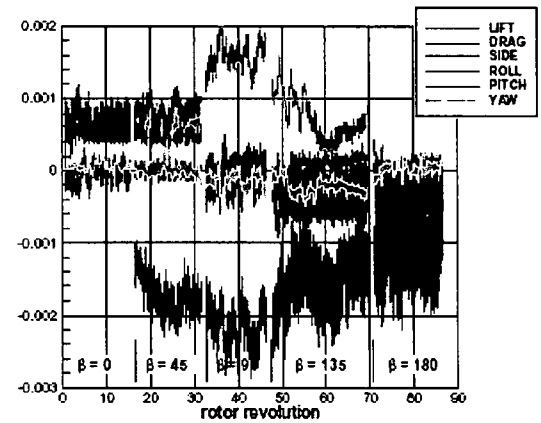

Figur 7. OVERFOW-D airframe coefficient time histories as a function of wind azimuth, 35-knot wind

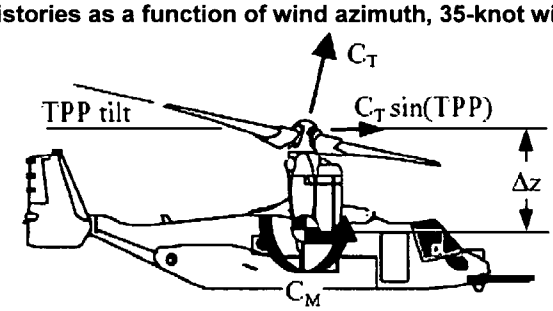

Figure 8. Definition of equivalent time path plane (TTP) tilt

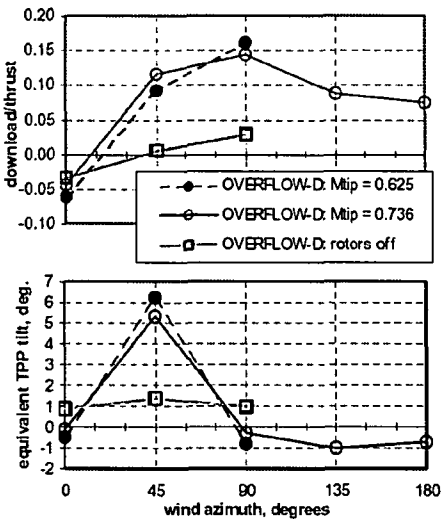

Figure 9. OVERFLOW-D time-averaged airframe DL/T and equivalent TTP tilt, 35-knot wind

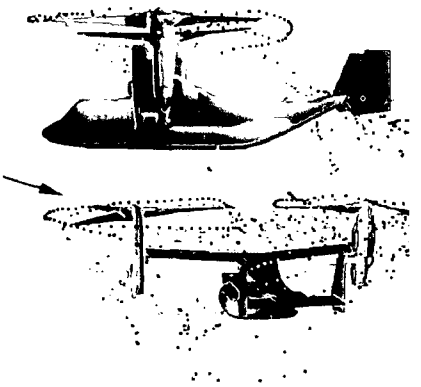

Figure 10. OVERFLOW-D time-dependent particle traces. Particle released from upwind (left) blade tips impinge on tail, 35-knot wind at 45° azimuth (→), M_{tip} = 0.625.

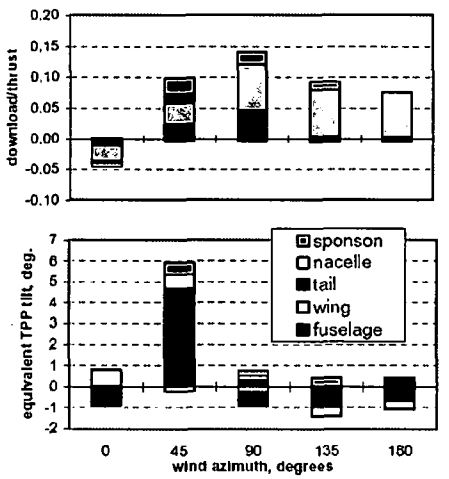

Figure 11. OVERFLOW-D time-averaged airframe DL/T and equivalent TPP tilt by airframe component, 35-knot wind

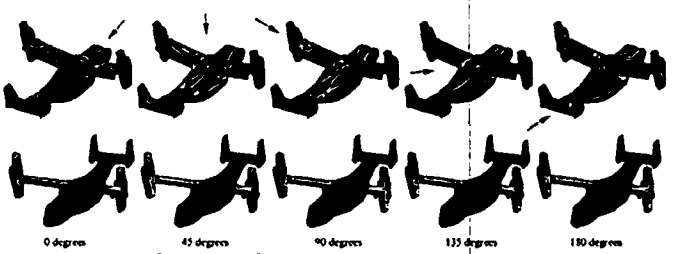

Figure 12. OVERFLOW-D instantaneous pressure force in download direction as a function of wind azimuth, 35-knot wind, blue – upload, red- download, black line – zero contour, arrow – wind direction

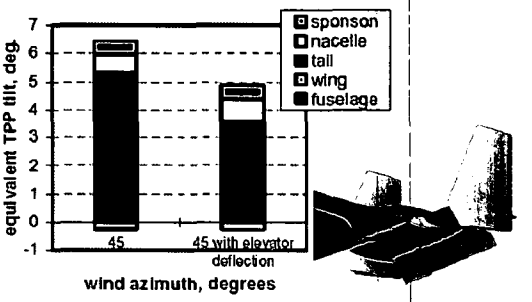

Figure 13. OVERFLOW-D effect of elevator deflection on PUWSS, M_{tip} = 0.625

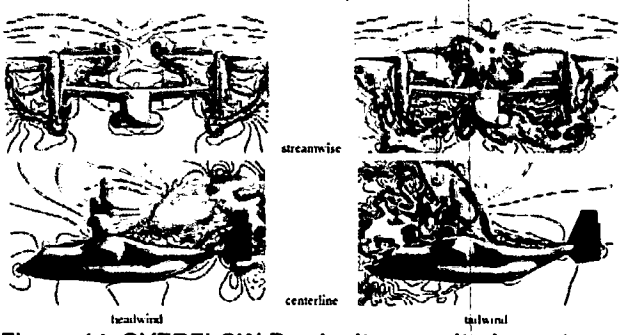

Figure 14. OVERFLOW-D velocity magnitude contours in a streamwise plane at the aircraft CG and a centerline plane, 35-knot head and tailwinds, blue – low, red – high